

# Moment Tensor Inversion for the 5 July 1930 Montilla Earthquake (Southern Spain)

J. Batlló,<sup>1</sup> D. Stich,<sup>2,3</sup> R. Macià,<sup>4</sup> and J. Morales<sup>2,3</sup>

## INTRODUCTION

The Iberia-Maghreb region, made up of Spain, Portugal, Algeria, and Morocco as well as the surrounding offshore areas in the Atlantic Ocean and Mediterranean Sea, is a complex plate boundary setting that displays important variations of earthquake faulting and stress patterns at regional and local scales (*e.g.*, Bufo *et al.* 2004; Stich *et al.* 2006; Fernández-Ibáñez *et al.* 2007; De Vicente *et al.* 2008). The inventory of seismic moment tensors for the Iberia-Maghreb region is rapidly increasing as the network of seismic broadband stations is becoming denser, and small-to-moderate earthquakes can now be included in the analysis. Automated near real-time moment tensor inversion is implemented at the Instituto Geográfico Nacional (IGN) (Rueda and Mézcua 2005), and the Instituto Andaluz de Geofísica (IAG) publishes processed moment tensor solutions, currently providing the largest regional catalog with 225 solutions to data (Stich *et al.* 2010). IAG source estimates are mainly for earthquakes since the mid 1990s; several older estimates (since 1980) can be found within routine larger-scale initiatives like the global CMT catalog (Dziewonski and Woodhouse 1983).

A less routine effort is source parameter retrieval from analog records for Iberia-Maghreb earthquakes that predate the era of digital seismogram recordings in order to supply faulting parameters and seismic moment for those historic earthquakes, particularly relevant for seismic hazard and/or seismotectonic studies (Pondrelli *et al.* 1999; Stich, Batlló *et al.* 2003; Stich *et al.* 2005; Batlló, Stich, Palombo *et al.* 2008). Here we report on source parameter retrieval for a damaging earthquake that struck the town of Montilla (near Córdoba, southern Spain) the night of 5 July 1930. The magnitude estimate for this earthquake is  $M_s = 5.1$  (Kárník 1969), and its epicentral intensity  $I_0$  has been evaluated as VIII (MSK). Just two contemporary studies describe this earthquake (Carbonell 1930; Navarro-Neumann 1931), both dealing with macroseismic effects. The macroseismic map was drawn by Rodriguez Navarro and is published in its original form in Galbis (1940)

and in an abridged form in Mezcua (1982). Unfortunately, the original questionnaires have been lost, and an updated review of the macroseismic field is not possible.

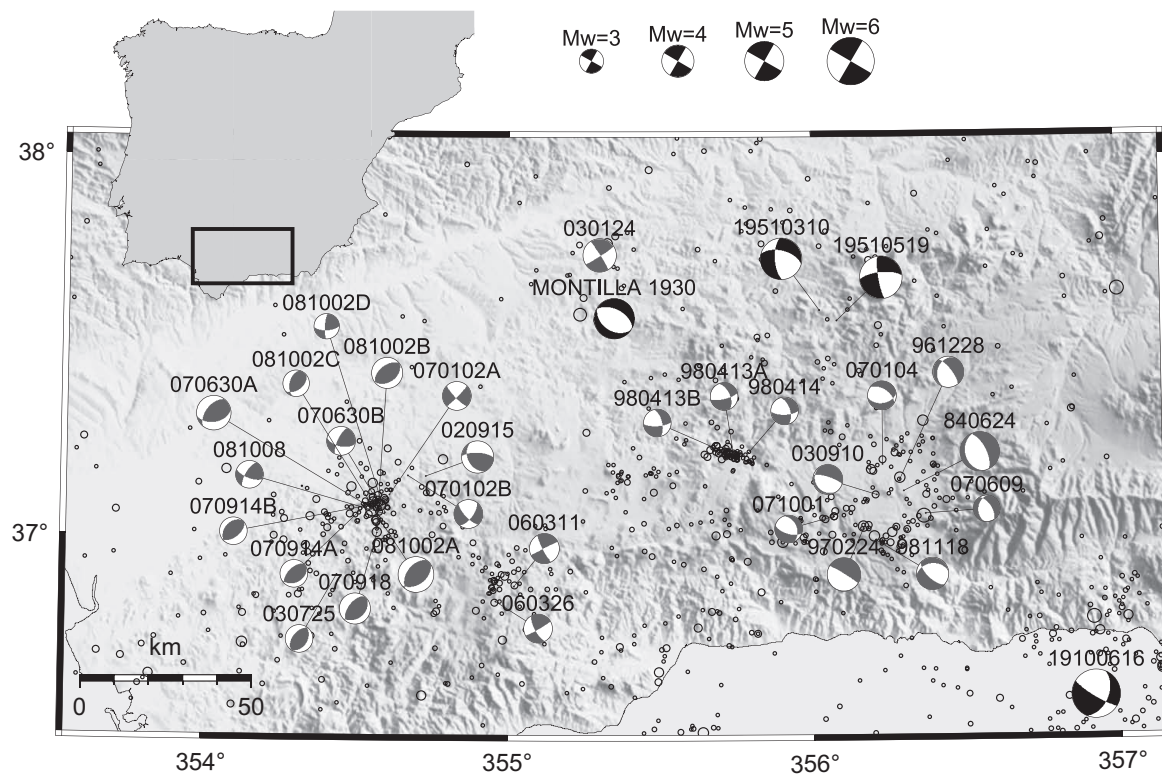
The 1930 Montilla earthquake is of moderate size, but still is the largest event recorded instrumentally in this area, situated in a gap between more seismically active areas to the east and west. This makes the event important to understanding regional tectonics and seismicity, since it may provide the missing link to characterize the transition between fundamentally different faulting patterns in the central and western Betic Cordillera. Aside from its regional significance, analysis of available seismograms represents an interesting case history of pushing the magnitude threshold for early 20th-century source inversion: Available near-regional seismograms (~200–700 km epicentral distance) are smoked paper recordings from medium-period, mechanical instruments with low gain and low resolution throughout, and are particularly challenging to digitize. Available recordings from electromagnetic instruments are all from distances around 1,500 km. The question is, how useful can these seismograms be for our purposes. The answer will provide clues for the study of events elsewhere with similar characteristics.

Here we describe our strategy to extract digital waveforms from these problematic recordings; relocate the source from information gathered in preserved seismograms, bulletins, and related contemporary documents; and use recovered waveforms for a regional moment tensor inversion. Two minor but crucial modifications are introduced compared to standard moment tensor schemes: 1) we will circumvent deconvolution of the instrument response (Rivera *et al.* 2002); and 2) we will process original horizontal waveforms without rotation into a cylindrical ray-coordinate system (Stich *et al.* 2005).

## REGIONAL SEISMICITY AND GEOLOGY

Seismic activity in the western part of the Eurasian-African (Nubia) plate boundary (Gulf of Cadiz/south of the Iberian Peninsula/north of Africa), is the consequence of oblique plate convergence with a NW-SE to WNW-ESE direction and rate of around 4–5 mm/year (*e.g.*, DeMets *et al.* 1994; Calais *et al.* 2003; Serpelloni *et al.* 2006). Coeval extension in the context of the opening of the western Mediterranean (Faccenna *et al.* 2004) can be observed, for example, in the Alboran Sea, significantly complicating the tectonics of the region.

1. Universidade de Lisboa, Lisbon, Portugal
2. Instituto Andaluz de Geofísica, Granada, Spain
3. Departamento de Física Teórica y del Cosmos, Universidad de Granada, Spain
4. Dept. Matemàtica Aplicada II, Universitat Politècnica de Catalunya, Barcelona, Spain



▲ **Figure 1.** Seismicity of the central Guadalquivir Valley, site of the 1930 earthquake. All known focal mechanisms obtained from moment tensor analysis are plotted. Gray beach balls correspond to inversion of modern broadband waveforms. Black beach balls are those obtained from digitization and inversion of old analog records (Stich, Batlló, *et al.* 2003; Stich *et al.* 2005; Batlló, Stich, Palombo *et al.* 2008).

Within southern Spain's Betic Cordillera, seismicity is characterized by low-to-moderate magnitudes ( $M < 5.5$ ) and is diffusely distributed (Figure 1). Most earthquakes are located in the shallow brittle crust ( $< 20$  km), except for intermediate-depth seismicity at the Malaga coast, which reaches depths of about 120 km (Buforn *et al.* 1995; Serrano 1999). The pattern of focal mechanisms in the Betic Cordillera changes from east to west. Predominately strike-slip faulting with an approximately  $N35^{\circ}E$  orientation of the maximum compressive stress  $\sigma_1$  is observed in the eastern part of the Betic Cordillera and in the trans-Alboran shear zone that connects the Spanish and Moroccan margins of the Alboran Sea with overall  $N45E$  strike (Stich *et al.* 2006). Farther west, we observe predominately normal faulting mechanisms in the central Betics, generally in geographical proximity to Neogene intramountain basins, indicating ENE-WSW extension (Galindo-Zaldívar *et al.* 1999). Finally, in the western Betics and southwestern Iberian Peninsula, we observe reverse and strike-slip faulting. While the orientations of strike-slip mechanisms appear heterogeneous, the reverse faulting solutions correspond to NW-SE compression, subparallel to the direction of plate convergence (Ruiz-Constán *et al.* 2009; Stich *et al.* 2010).

Within this general context, the 1930 Montilla earthquake is located between the realm of normal faulting mechanisms in the central Betics and the compressive deformation in the western Betics, and we have no clue about which type of focal mechanism to expect. A nearby magnitude 4 earthquake in 2003

yields a pure strike-slip faulting solution (Stich *et al.* 2006), but a comparison of waveforms between 1930 and 2003 (using, for example, station SFS or the nearby TOL/PAB recordings) indicates that the events were not similar. The town of Montilla is located in the southernmost part of the Guadalquivir Valley, not far from the external thrust front of the Betic chain. The Guadalquivir basin is an asymmetric, Neogene foreland basin filled with several types of sediments and formed by the load of the Betic Cordillera over the Iberian Variscan massif foreland (García-Castellanos *et al.* 2002). The Variscan massif located to the north of the Guadalquivir basin penetrates to the south, forming the basement beneath the basin and also beneath the alpine thrust sheets of the Betic Cordillera.

## SEISMOGRAM DIGITIZATION

A thorough search for seismograms of the 1930 Montilla earthquake led to the collection of 47 records from 18 seismic stations. The databank of the EUROSEISMOS project (Ferrari and Pino 2003; Michelini *et al.* 2005) has been extremely useful and provided us with more than half of the collected seismograms. Most of them are recorded on smoked paper (TOL, SFS, ALM, EBR, FBR, COI, MNH). Let us remember that signals of  $M \sim 5$  earthquakes recorded at mechanical seismographs on smoked paper (amplification around 200; free period near 10 s) vanish for stations located at distances more than  $\sim 1,500$  km. Electromagnetic instruments (amp. 1,000;

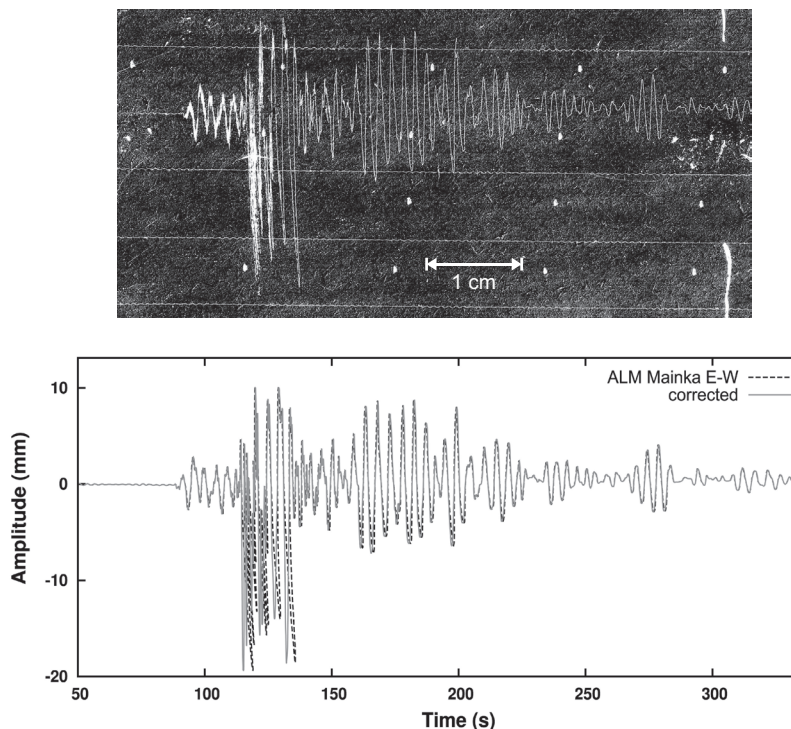
**TABLE 1**

List of selected seismograms with the collected instrumental constants of the recording instruments and its conversion to poles and zeroes as explained in Batlló (2004). Columns are, for mechanical seismographs: 1) Sta.: Station name, 2) Instr.: Seismograph's name, 3) Comp.: recording component, 4) To: Free period of the mechanical sensor, 5) Damp.: Sensor damping, 6) Gain: Instrument magnification, 7) Zeroes: Zeroes of the instrument response function, 8) Poles: Poles of the instrument response function. For the electromagnetic seismographs, same as before except columns 4) To S.: Free period of the electromagnetic sensor and 5) To G.: Free period of the recording galvanometer.

MECHANICAL SEISMOGRAPHS							
Sta.	Instr.	Comp.	To	Damp.	Gain	Zeroes	Poles
ALM	Mainka	E–W	4.8	0.30	238.	0.0, 0.0 (double)	–0.393, ±1.249
ALM	Mainka	N–S	9.4	0.30	303.	0.0, 0.0 (double)	–0.201, ±0.638
ALM	Mainka	Z	6.0	0.30	141.	0.0, 0.0 (double)	–0.314, ±0.999
COI	Wiechert	E–W	10.4	0.36	245.	0.0, 0.0 (double)	–0.217, ±0.564
COI	Wiechert	N–S	10.7	0.35	258.	0.0, 0.0 (double)	–0.206, ±0.550
SFS	Graiño	N–S	13.0	0.20	90.	0.0, 0.0 (double)	–0.097, ±0.474
TOL	Wiechert	NE–SW	15.0	0.45	250.	0.0, 0.0 (double)	–0.188, ±0.374
MNH	Wiechert	E–W	12.5	0.40	240.	0.0, 0.0 (double)	–0.201, ±0.461
MNH	Wiechert	N–S	12.5	0.40	240.	0.0, 0.0 (double)	–0.231, ±0.446
ELECTROMAGNETIC SEISMOGRAPHS							
Sta.	Instr.	Comp.	To S.	To G.	Gain	Zeroes	Poles
DBN	Galitzin	E–W	25.0	25.0	247.	0.0, 0.0 (triple)	0.251, 0.0 (quadruple)
DBN	Galitzin	N–S	25.0	25.0	247.	0.0, 0.0 (triple)	0.251, 0.0 (quadruple)
DBN	Galitzin	Z	12.0	12.0	1193.	0.0, 0.0 (triple)	0.524, 0.0 (quadruple)
KEW	Galitzin	E–W	24.7	24.8	273.	0.0, 0.0 (triple)	0.254, 0.0 (double) 0.253, 0.0 (double)
KEW	Galitzin	N–S	25.5	24.7	294.	0.0, 0.0 (triple)	0.246, 0.0 (double) 0.254, 0.0 (double)
KEW	Galitzin	Z	13.0	13.0	685.	0.0, 0.0 (triple)	0.483, 0.0 (quadruple)
STR	Galitzin	E–W	22.2	22.2	526.	0.0, 0.0 (triple)	0.283, 0.0 (quadruple)
STR	Galitzin	N–S	22.4	22.4	567.	0.0, 0.0 (triple)	0.280, 0.0 (quadruple)
STR	Galitzin	Z	11.6	11.6	1128.	0.0, 0.0 (triple)	0.542, 0.0 (quadruple)
UCC	Galitzin	E–W	24.5	24.4	670.	0.0, 0.0 (triple)	0.256, 0.0 (double) 0.258, 0.0 (double)
UCC	Galitzin	N–S	24.0	24.5	694.	0.0, 0.0 (triple)	0.262, 0.0 (double) 0.256, 0.0 (double)
UCC	Galitzin	Z	8.0	1.5	1550.	0.0, 0.0 (triple)	0.785, 0.0 (double) 0.546, 0.0 (double)

free period 10–20 s approx.) can record such an earthquake up to ~3,000 km. This is the case for the records at KEW, STR, DBN, and UCC. Records for stations TOL and SFS were obtained from contemporary printed reproductions published in journals. They were rescaled to the original size of the record sections using the distance between time marks and our information about the paper speed of the recording instruments (Batlló 2004). It was quite common at that time to “enhance” the trace for further reproduction by just redrawing on top of it with a pen. This is the case for the TOL and SFS records, and especially in the case of SFS the reproduced traces do not fit exactly the recorded traces. Records for station STR were recovered from microfilm.

Disregarding seismograms that were not suitable for digitization because the trace could not be followed reliably or the recordings showed evident instability, we finally digitized 23 waveforms from 10 recording stations. Some records were rejected because it was impossible to distinguish the consecutive swings of the recording stylus. This was the case, for example, at station MAL, 100 km from the epicenter. Table 1 gives the list of selected seismograms with the collected instrumental constants of the seismographs (mostly from Batlló 2004 and the EUROSEISMOS project). The original seismograms were scanned and manually digitized using AUTOCAD, following the procedure described in Batlló *et al.* (1997). The digitized records were corrected for trace curvature due to the



▲ **Figure 2.** (Top) ALM Mainka E-W component seismogram, scanned from the original on smoked paper. The station lies 210 km away from the epicenter at azimuth  $113^\circ$ . Note that the original width of the seismogram fragment is just 7 cm long (horizontal and vertical scales are equal). (Bottom) The raw digitized seismogram (black dashed line) with the corrected trace on top (gray line).

finite length of the recording arm and for skew, as described in Batlló, Stich, and Macià (2008), but problems appeared when removing the curvature introduced by the recording arm's finite length and the trace skew. A careful analysis showed that these problems were not due to mistakes in the manual digitization but to low resolution of the image due to the absolute dimensions of the whole seismogram. The recording of high-frequency motion at relatively low drum speed poses a formidable problem, especially at the nearest seismic stations.

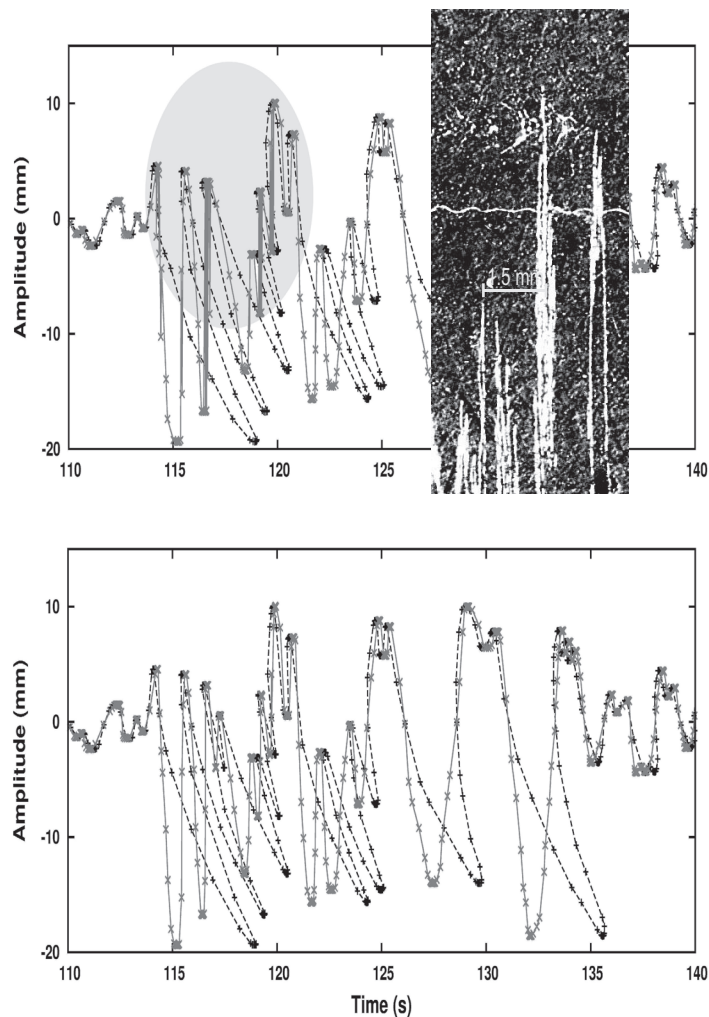
We show an example of digitizing problems for the ALM Mainka seismograph E-W trace (see Figures 2 and 3). The width of the trace, measured on the original seismogram, is 0.1 mm, and the recording speed 15 mm/min. Visual inspection of body waves shows recorded oscillations with 1-Hz frequency and (double) amplitudes up to 25 mm. In such a case even an accurate digitization of the trace shows serious problems for maintaining the order of acquired points once corrected. This is not due to digitization errors but rather to the particular conditions of the records under study. Taking a look at the real dimensions of the recorded signal, we realized that an oscillation with a frequency of 1 Hz on such a seismogram is just  $\frac{1}{4}$  mm wide, translating into a ratio of horizontal vs. vertical dimensions of the swing of  $\sim 1/50$ . In such cases, the smallest lateral twisting or oscillation of the axis of the recording arm introduces lateral perturbations of the recorded traces that are greater than our resolution. On comparing the original seismograms with the digital images, traces of 0.1 mm width in images digitized at 1,016 dpi have a minimum width of 4 pixels, each pixel being 0.025 mm x 0.025 mm in real size. The solution to the problem

of the order of points requires moving the trace within a single pixel: we observed that moving the position of two consecutive digitized points within the width of a pixel alters its final order after corrections have been applied. Clearly, we are at the extreme limit of resolution for such seismograms.

As we are interested in recovering these records for waveform inversion, we decided to use them anyway. In such cases, the procedure to obtain a useful record is a slow, iterative process. The problematic points are “recentered” manually on the recorded trace, and the whole trace is corrected again for arm length and skew and scrutinized for “misplaced” points. This procedure is iterated as many times as necessary. For some records just a few points are misaligned; TOL Wiechert NE-SW or ALM Mainka N-S were properly recovered after five such iterations. But for some records, ALM Mainka E-W or SFS Graiño N-S, for example, 14 and 26 iterations, respectively, were necessary. As the procedure takes a long time it is clear that we can hardly afford to use it for “any” record, but we can apply it to selected records, in our case for the nearest stations to the epicenter and for stations that reduce the azimuthal gap by more than half.

## LOCATION AND MOMENT TENSOR SOLUTION

Available instrumental locations for the 1930 earthquake place it near the town of Montilla ( $37^\circ 37'N$ ,  $4^\circ 38'W$ , Mezcua and Martínez-Solares 1983), consistent with the occurrence of the largest macroseismic effects. Nevertheless, prior to moment tensor calculation, and to avoid bias, we relocated the earthquake



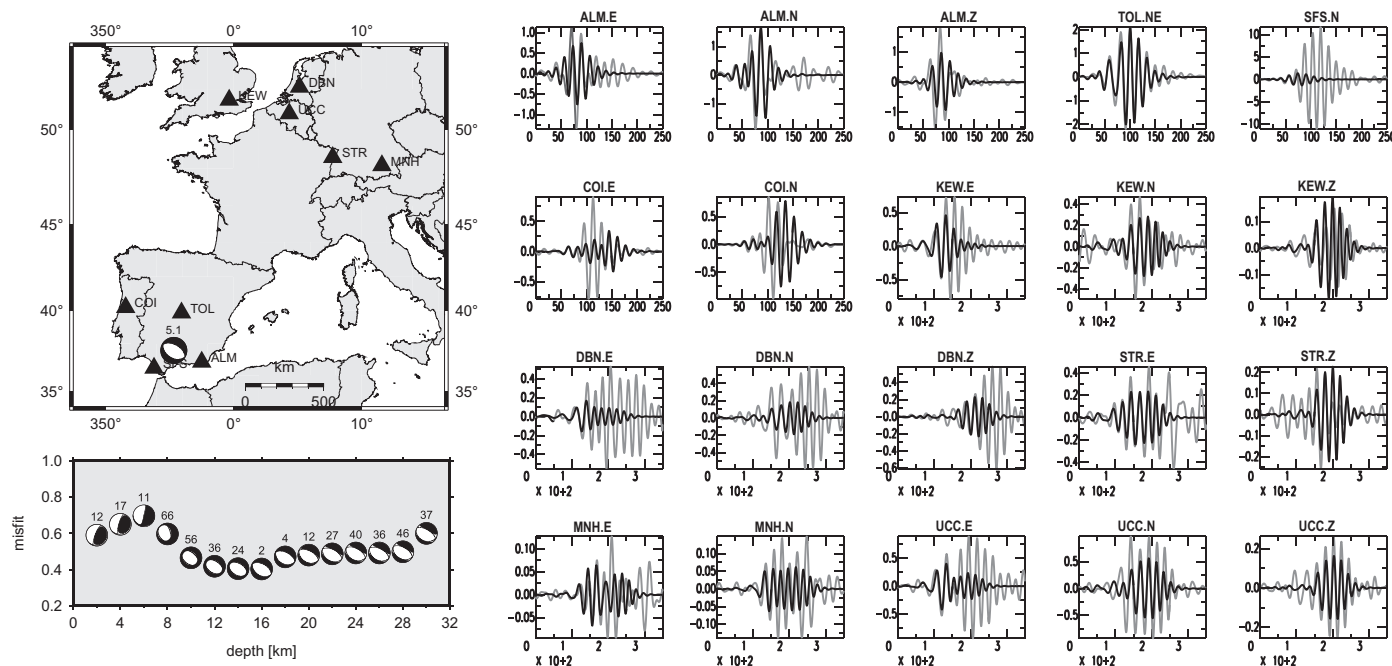
▲ **Figure 3.** (Top) *S* waves from Figure 2 look properly corrected, but if the image is enlarged problems appear. The gray oval shows digitized peaks corresponding to those marked by the scale shown on the seismogram fragment to the right. The digitized points (black dashed line) are out of order (gray line) after correction. Note that here the images are greatly enlarged. In the real seismogram we are dealing with 1.5 mm (6 s) of record as marked on the right image. (Bottom) After 14 iterations of correcting mismatched points and scrutinizing the results, we obtained a useful digitized trace.

based on the contemporaneous documents we were able to collect. We use the original bulletins and waveforms to crosscheck the arrival times provided by the International Seismological Summary (ISS) bulletin. Location was performed with the program HYPOCENTER (Lienert and Havskov 1995), using a global (IASPEI 91) as well as a regional earth model (Stich, Ammon *et al.* 2003). We locate the earthquake at  $37^{\circ} 33.8'N$ ,  $4^{\circ} 38.1'W$ ,  $h = 7.7$  km in the global model and at  $37^{\circ} 33.4'N$ ,  $4^{\circ} 38.7'W$ ,  $h = 0.0$  km in the local model. The obtained results do not show any large deviation from the previously reported location and confirm the available epicenter estimates. We obtained confidence limits, previously unavailable, of 15.5 km on longitude and 11.9 km on latitude, defining the epicenter quality.

We use the location  $37^{\circ} 33.4'N$ ,  $4^{\circ} 38.7'W$  for full-waveform, time-domain inversion of the deviatoric moment tensor, minimizing the least-squares misfit between synthetic moment tensor predictions and observed waveforms. Green's functions

are computed for a layered earth model originally developed for the Iberian Peninsula (Stich, Ammon *et al.* 2003) that provides a reasonable approximation to the continental crust in western Europe and was successfully applied to correct propagation effects for other earthquakes in southern Spain recorded at western and central European stations (Batlló, Stich, Palombo *et al.* 2008). We align Green's functions and recorded waveforms at the *P* arrival. We repeat moment tensor inversion for different trial depths with increments of 2 km in search of the global misfit minimum, in order to avoid bias by the poorly constrained source depth from the relocation results. A more detailed description of the inversion procedure is given in Stich, Ammon, *et al.* (2003).

We adapted moment tensor inversion to better deal with old traces by introducing the rotation of the horizontal Green's functions instead of the recorded seismograms, the latter being processed in the original sensor orientations (Stich *et al.* 2005). In this way we can use single components such as SFS and TOL



▲ **Figure 4.** (Left) Map showing the location of the stations used for the inversion and the focal mechanism obtained. The depth fitting is shown at bottom. Small numbers above beach balls indicate the non-double-couple (CLVD) component. (Right) Fit of the recorded waveforms (gray) and the modeled seismograms (black). Units are seconds and mm, with amplitudes referring to bandpass-filtered uncorrected original recordings since no deconvolution is involved in processing. Note that the *P*-wave train on the three components of ALM and the unique component of SFS (on top) fit the theoretically calculated waveforms (black) quite well.

and reduce the problems introduced by uncertainties of the instrument response or the misalignment of time signals from component to component. A second modification compared to standard moment tensor schemes is the application of the instrument response to the Green's functions (through convolution) instead of deconvolving the response from the recorded waveforms (Kikuchi *et al.* 2003). Deconvolution was found to be unstable for several recordings, presumably due to long-period distortions such as baseline instabilities. This procedure reduces the effective bandwidth in a least-squares scheme and requires additional weighting factors to compensate for the different amplifications of the recording systems during inversion, but it allows using the original recovered waveforms as unaltered as possible. The only operation performed on digitized seismograms prior to inversion is a bandpass filter for periods from 20 s to 50 s for far-regional stations (distances > 1,000 km), and from 15 s to 35 s for stations in the Iberian Peninsula.

The moment tensor inversion achieves good or reasonable fits to the observed seismograms (Figure 4), supporting a pure normal faulting mechanism for this earthquake. Nodal planes have orientations of  $123^{\circ}/39^{\circ}/-86^{\circ}$  (strike/dip/rake) and  $298^{\circ}/51^{\circ}/-93^{\circ}$ , with a near vertical *P* axis at  $188^{\circ}/83^{\circ}$  (strike/plunge) and near horizontal *T* axis at  $30^{\circ}/6^{\circ}$ . The non-double-couple (CLVD) component of the inverted moment tensor is small (2% CLVD). Formally the best hypocentral depth is 16 km; however this parameter is not tightly constrained. The moment magnitude is  $M_w = 5.1$  and seismic moment  $5.48 \times 10^{16}$  Nm. The quality of recovered waveforms and waveform fits at the far-regional electromagnetic instruments (KEW, STR,

DBN, UCC) is comparable to the case of the nearby 1951 Jaén earthquakes (Batlló, Stich, Palombo *et al.* 2008), with 1.46 and 2.12 times larger moment release and similar source depth. This confirms that source inversion for historic magnitude 5 earthquakes can be addressed using far-regional Galitzin recordings. Finally, we stress that the three components of the Mainka instrument at ALM and the single Graiño N-S record from SFS, which are among our most problematic records and were digitized using iterative trace recentering at sub-pixel resolution, achieve quite a good fit for the modeled body waves. After dedicated preprocessing, these near-distance traces proved useful for source inversion, in our case significantly reducing the azimuthal gap. At SFS, while the *P*-arrival matches well, surface waves show major discrepancies compared to the moment tensor prediction. This is apparently due to the combination of a very low damping of the instrument and particular propagation effects at SFS station for northeastern backazimuths, where a severe underprediction of intermediate-period surface waves is also observed for modern broadband recordings (Mancilla *et al.* 2002; Stich, Ammon *et al.* 2003).

## CONCLUSIONS

We confirmed the epicentral location of the 5 July 1930 earthquake near Montilla from a revised set of phase arrival data and computed the seismic moment tensor from manually digitized seismograms. The earthquake can be attributed to pure normal faulting on a WNW-ESE trending fault. Although due to a lack of mechanisms in the source area we had no real clues

about what type of focal mechanism to expect, the solution for the 1930 earthquake comes as a bit of a surprise. The closest moment tensor solutions show strike-slip faulting, and the earthquake is situated close to the external thrust front of the Betic chain, but the obtained normal faulting solution is rather similar to earthquakes located around the Granada basin 80 to 100 km to the southeast, in the internal zone of the mountain range. We computed a moment magnitude of 5.1, confirming that this is a significant earthquake in the context of regional seismicity. This permits us to hypothesize that the 1930 faulting mechanism is representative of the tectonic deformation in this area. Under this hypothesis, mid-crustal normal faulting in proximity to the Betic thrust front suggests that this sector of the mountain front is not active (Ruiz-Constán *et al.* 2009), and the transition to the compressive regime at the western Betic mountain front should be located farther west, roughly around 5°W. While the faulting style is remarkable, the *P* and *T* axes orientations follow the regional pattern (De Vicente *et al.* 2008), providing support that the 1930 earthquake is probably not the result of a local perturbation of the stress field.

In addition to the intrinsic interest in this earthquake, this analysis provided a good opportunity to explore the limits of historical seismogram analysis, considering the low magnitude of the event. The result is encouraging and confirms that magnitude 5 earthquakes can be analyzed when we take special care with the digitization. At the same time, the difficulties we encountered show that we have pushed the methodology close to its limit, and it will become extremely difficult to analyze earthquakes with  $M < 5$  from such kinds of records. For electromagnetic instruments situated at around 1,500 km distance, smaller events cannot be expected to provide sufficient resolution for intermediate-period waves (although shorter station distances may even permit the analysis of magnitude 4.5 earthquakes; see Dreger and Savage 1999). For near-regional mechanical seismographs with smoked paper recording, our study confirmed that it is possible to use almost undamped records, at least for body waves, but the limit is tied to frequency resolution and depends on the distance. The closest recordings, 100 km from the epicenter, had to be discarded because high-frequency ground oscillations overwrite each other on the seismograms. For other stations at ~200 km from the epicenter we observe highly problematic records, but we were able to extract suitable digital waveforms using a manual, iterative scheme where we repeatedly recentered the trace within single pixels until we recovered the correct temporal order of points. This inefficient strategy can hardly be applied routinely, but here it proved useful for including some of the most relevant recordings that could not be digitized with standard sequential processing schemes. ☒

## ACKNOWLEDGMENTS

We are grateful to all individuals and institutions that participate in the effort to preserve old analog seismograms and for making these seismograms available to us. We received financial support from the Spanish DGI Projects Numbers

CGL2008-01830 and P09-RNM-5100 and Project Consolider TopoIberia CSD2006-00041.

## REFERENCES

- Batló, J. (2004). *Catálogo—Inventario de Sismógrafos Antiguos Españoles*. Madrid: Instituto Geográfico Nacional, 414 pps.
- Batló, J., D. Stich, and R. Macià (2008). Quantitative analysis of early seismograph recordings. In *Historical Seismology: Interdisciplinary Studies of Past and Recent Earthquakes*, ed. J. Fréchet, M. Meghraoui, and M. Stucchi, 379–396. Berlin: Springer Verlag.
- Batló, J., D. Stich, B. Palombo, R., Macià, and J. Morales (2008). The 1951 *M<sub>w</sub>* 5.2 and 5.3 Jaén, southern Spain, earthquake doublet revisited. *Bulletin of the Seismological Society of America* **98**, 1,535–1,545.
- Batló, J., T. Susagna, and A. Roca (1997). A processing system for old records of regional earthquakes: Analysis of the 19th November 1923 earthquake in the Pyrenees. *Cahiers du Centre Européen de Géodynamique et de Séismologie* **13**, 149–157. In English.
- Bufo, E., M. Bezzeghoud, A. Udías, and C. Pro (2004). Seismic sources on the Iberia-African plate boundary and their tectonic implications. *Pure and Applied Geophysics* **161**, 623–646.
- Bufo, E., C. Sanz de Galdeano, and A. Udías (1995). Seismotectonics of the Ibero-Maghrebian region. *Tectonophysics* **248**, 247–261.
- Calais, E., C. DeMets, and J. M. Nocquet (2003). Evidence for a post-3.16-Ma change in Nubia–Eurasia–North America plate motions? *Earth and Planetary Science Letters* **216**, 8–92.
- Carbonell, A. (1930). El terremoto de Montilla (5 Julio 1930). *Boletín del Instituto Geológico y Minero de España* **52**, 293–331.
- De Vicente, G., S. Cloetingh, A. Muñoz-Martín, A. Olaiz, D. Stich, R. Vegas, J. Galindo-Zaldívar, and J. Fernández-Lozano (2008). Inversion of moment tensor focal mechanisms for active stresses around the microcontinent Iberia: Tectonic implications. *Tectonics* **27**, doi:10.1029/2006TC002093.
- DeMets, C., R. G. Gordon, D. F. Argus, and S. Stein (1994). Effect of recent revisions to the geomagnetic reversal time scale on estimates of current plate motions. *Geophysical Research Letters* **21**, 2,191–2,194.
- Dreger, D., and B. Savage (1999). Aftershocks of the 1952 Kern County, California, earthquake sequence. *Bulletin of the Seismological Society of America* **89**, 1,094–1,108.
- Dziewonski, A. M., and J. H. Woodhouse (1983). An experiment in the systematic study of global seismicity: Centroid moment-tensor solutions for 201 moderate and large earthquakes of 1981. *Journal of Geophysical Research* **88**, 3,247–3,271.
- Faccenna, C., C. Piromallo, A. Crespo Blanc, L. Jolivet, and F. Rossetti (2004). Lateral slab deformation and the origin of the arcs of the western Mediterranean. *Tectonics* **23**, doi:10.1029/2002TC001488.
- Ferrari, G. and N. A. Pino (2003). EUROSEISMOS 2002–2003. A project for saving and studying historical seismograms in the Euro-Mediterranean area. *Geophysical Research Abstracts* **5**, 05274.
- Fernández-Ibáñez, F., J. I. Soto, M. D. Zoback, and J. Morales (2007). Present-day stress field in the Gibraltar Arc (western Mediterranean). *Journal of Geophysical Research* **112**, B08404; doi:10.1029/2006JB004683.
- Galbis, J. (1940). *Catálogo sísmico de la zona comprendida entre los meridianos 5° E y 20° W y paralelos 45° y 25° N*. Madrid: Tomo II, Inst. Geográfico y Catastral, 277 pps.
- Galindo-Zaldívar, J., A. Jabaloy, I. Serrano, J. Morales, F. González-Lodeiro, and F. Torcal (1999). Recent and present-day stresses in the Granada Basin (Betic Cordilleras): Example of a late Miocene–present-day extensional basin in a convergent plate boundary. *Tectonics* **18**, 686–702.
- García-Castellanos, D., M. Fernández, and M. Torné (2002). Modeling the evolution of the Guadalquivir foreland basin (southern Spain). *Tectonics* **21** (3); doi:10.1029/2001TC001339.

- Kárník, V. (1969). *Seismicity of the European Area*. Vol. 1. Dordrecht, Holland: D. Reidel Publishing Co., 364 pps.
- Kikuchi, M., M. Nakamura, and K. Yoshikawa (2003). Source rupture processes of the 1944 Tonankai earthquake and the 1945 Mikawa earthquake derived from low-gain seismograms. *Earth Planets Space* **55**, 159–172.
- Lienert, B. R. E., and J. Havskov (1995). A computer program for locating earthquakes both locally and globally. *Seismological Research Letters* **66**, 26–36.
- Mancilla, F., C. J. Ammon, R. B. Herrmann, and J. Morales (2002). Faulting parameters of the 1999 Mula earthquake, southeastern Spain. *Tectonophysics* **354**, 139–155.
- Mezcua, J. (1982). *Catálogo general de isosistas de la Península Ibérica*. Publication 202. Madrid: Instituto Geográfico Nacional, 61 pps. + 261 plates.
- Mezcua, J., and J. M. Martínez Solares (1983). *Sismicidad del área Iberomagrebi*. Publication 203. Madrid: Instituto Geográfico Nacional, 301 pps.
- Michelini, A., B. De Simoni, A. Amato, and E. Boschi (2005). Collecting, digitizing and distributing historical seismological data. *Eos, Transactions, American Geophysical Union* **86** (28), 261.
- Navarro-Neumann, M. M. S. (1931). Notas sismológicas del año 1930. *Ibérica* **35**, 310–318.
- Pondrelli, S., G. Ekström, A. Morelli, and S. Primerano (1999). Study of source geometry for tsunamigenic events of the Euro-Mediterranean area. In *International Conference on Tsunamis*, 297–307. Paris: UNESCO Books.
- Rivera, L., K. Sieh, D. Helmberger, and D. Natawidjaja (2002). A comparative study of the Sumatran subduction-zone earthquakes of 1935 and 1984. *Bulletin of the Seismological Society of America* **92**, 1,721–1,736.
- Rueda, J., and J. Mézcua (2005). Near-real-time seismic moment-tensor determination in Spain. *Seismological Research Letters* **76**, 455–465.
- Ruiz-Constán, A., D. Stich, J. Galindo-Zaldívar, and J. Morales (2009). Is the northwestern Betic Cordillera mountain front active in the context of the convergent Eurasia-Africa plate boundary? *Terra Nova* **21**, 352–359.
- Serpelloni, E., G. Vannucci, S. Pondrelli, A. Argñani, G. Casula, M. Anzidei, P. Baldi, and P. Gasperini (2007). Kinematics of the Western Africa–Eurasia plate boundary from focal mechanisms and GPS data. *Geophysical Journal International* **169**, 1,180–1,200.
- Serrano, I. (1999). Distribución espacial de la sismicidad en las Cordilleras Béticas-Mar de Alborán. Ph.D. thesis, Universidad de Granada, Spain, 231 pps.
- Stich, D., C. J. Ammon, and J. Morales (2003). Moment tensor solutions for small and moderate earthquakes in the Ibero-Maghreb region. *Journal of Geophysical Research* **108**, (B3). doi: 10.1029/2002JB002057
- Stich, D., J. Batlló, R. Macià, P. Teves-Costa, and J. Morales (2005). Moment tensor inversion with single-component historical seismograms: The 1909 Benavente (Portugal) and Lambesc (France) earthquakes. *Geophysical Journal International* **162**, 850–858.
- Stich, D., J. Batlló, J. Morales, R. Macià, and S. Dineva (2003). Source parameters of the 1910  $M_w = 6.1$  Adra earthquake (southern Spain). *Geophysical Journal International* **155**, 539–546.
- Stich, D., R. Martín, and J. Morales (2010). Moment tensor inversion for Iberia-Maghreb earthquakes 2005–2008. *Tectonophysics* **48**, 390–398.
- Stich, D., E. Serpelloni, F. Mancilla, and J. Morales (2006). Kinematics of the Iberia-Maghreb plate contact from seismic moment tensors and GPS observations. *Tectonophysics* **426**, 295–317.

*Universidade de Lisboa*  
*Instituto D. Luiz-CGUL*  
*Campo Grande, Edifício C8*  
*1749-016 Lisbon, Portugal*  
*jobatll@fc.ul.pt*  
*(J. B.)*

*Instituto Andaluz de Geofísica & Dept. de Física Teórica y del Cosmos*  
*Universidad de Granada*  
*Campus Universitario de Cartuja s/n*  
*E-18071 Granada, Spain*  
*daniel@iag.ugr.es*  
*(D. S.)*  
*morales@iag.ugr.es*  
*(J. M.)*

*Dept. Matemàtica Aplicada II*  
*Universitat Politècnica de Catalunya,*  
*Pla de Palau 18*  
*E-08003 Barcelona, Spain*  
*ramon.macia@upc.edu*  
*(R. M.)*